

SUPPORTING INFORMATION for:

Unprecedented Trapping of Difluorooctamolybdate Anions within an α -Polonium Type Coordination Network

Olena V. Sharga,^a Andrey B. Lysenko,^{a*} Marcel Handke,^b Harald Krautschied,^b Eduard B. Rusanov,^c Alexander N. Chernega,^c Karl W. Krämer,^d Shi-Xia Liu,^{d*} Silvio Decurtins,^d Adam Bridgeman,^e Konstantin V. Domasevitch^a

^a Inorganic Chemistry Department, Taras Shevchenko National University of Kyiv, Volodimirska Str. 64, Kyiv 01033, Ukraine

^b Institut für Anorganische Chemie, Universität Leipzig, Johannisallee 29, D-04103 Leipzig, Germany

^c Institute of Organic Chemistry, Murmanska Str. 5, Kyiv, 02660, Ukraine

^d Departement für Chemie und Biochemie, Universität Bern, Freiestrasse 3, CH-3012 Bern, Switzerland

^e School of Chemistry, The University of Sydney, NSW, 2006, Australia

- Corresponding authors. E-mail address: ab_lysenko@univ.kiev.ua (Lysenko A.B.), liu@iac.unibe.ch (Liu S.-X.)

	<i>Content</i>	<i>Page</i>
X-Ray refinements		3
Table S1.	Crystal data for complexes 1-3 .	4
Figure S1.	Crystal structure and labeling scheme for $[\text{Mo}_2\text{F}_2\text{O}_5(\text{tr}_2\text{pr})]$, (1).	5
Table S2.	Selected bond lengths (Å) and angles (°) for 1 .	5
Figure S2.	Illustration of a 2D H-bonding pattern in the crystal structure of $[\text{Mo}_2\text{F}_2\text{O}_5(\text{tr}_2\text{pr})]$, (1).	6
Figure S3.	Crystal structure and labeling scheme for $[\text{Co}_3(\text{tr}_2\text{pr})_2(\text{MoO}_4)_2\text{F}_2] \cdot 7\text{H}_2\text{O}$ (2).	6
Figure S4.	Illustration of the centrosymmetrical trinuclear fragments in the crystal structure 2 .	7
Table S3.	Selected bond lengths (Å) and angles (°) for 2 .	7-8
Figure S5.	The H-bonding patterns showing the interconnections between the neighboring $[\text{Co}_3(\text{tr})_4(\text{MoO}_4)_2\text{F}_2]_n$ chains.	9
Table S4.	Hydrogen bonding contacts in the crystal structure of 2 (Å, °).	9
Figure S6.	Illustration of the C-H...O and O-H...O(or F) contacts in the crystal structure 2 .	10
Figure S7.	Crystal structure and labeling scheme for $[\text{Co}_3(\text{H}_2\text{O})_2(\text{tr}_2\text{pr})_3(\text{Mo}_8\text{O}_{26}\text{F}_2)] \cdot 3\text{H}_2\text{O}$ (3).	11
Table S5.	Selected bond lengths (Å) and angles (°) for 3 .	12-16
Figure S8.	The O-H...F hydrogen-bonding interactions between coordinating water and $[\text{Mo}_8\text{O}_{26}\text{F}_2]^{6-}$ -anions (<u>O1</u> -H...F2 2.843(4) Å) in the crystal structure of 3 .	16
Figure S9.	Hydrogen-bonding interactions between non-coordinating water molecule and $[\text{Mo}_8\text{O}_{26}\text{F}_2]^{6-}$ -anions in the crystal structure of 3 .	16
Table S6.	Hydrogen bonding scheme in the crystal structure of 3 (Å, °).	17
Figure S10.	H-bonding patterns (O-H...O and O-H...F) in the crystal structure of 3 .	18
Figure S11.	Some weak C-H...O interactions in the crystal structure of 3 .	19
Figure S12.	Photographs of pink crystalline powder of compound 2 a); and orange powder of compound 3 b).	20
Figure S13.	Photographs of a step-wise separation process of compound 3 utilizing a flotation method in a $\text{CHBr}_3/\text{CHCl}_3$ solution	21
Figure S14.	IR spectra of complex 2 (KBr pellet).	22
Figure S15.	IR spectrum of complex 3 (KBr pellet).	22
Figure S16.	The powder XRD patterns of the unknown phase. (Anal. Found: C, 19.32; H 3.22; N, 18.88).	23
Figure S17.	The bulk-phase purity of complex 2 was confirmed by comparing its experimental and simulated XRPD patterns.	23
Figure S18.	The 2D and 3D Guinier-Simon diagrams of the TD-XRPD measurements of compound 2 .	24
Figure S19.	TG-MS analysis of complex 2 .	25
Figure S20.	The bulk-phase purity of compound 3 was confirmed by comparing the XRPD patterns with the simulated one.	25
Figure S21.	The 2D Guinier-Simon diagram of the TD-XRPD measurements of complex 3 .	26
Figure S22.	TG-MS analysis of complex 3 .	26
Figure S23.	Plot of $\chi_m(T)$ for 2 .	27
Figure S24.	Plot of $\chi_m(T)$ for 3 .	27

X-Ray refinements

CH hydrogen atoms were placed in calculated positions and refined as fixed contributions with $U_{\text{iso}}=1.2U_{\text{eq}}(\text{C})$, while OH hydrogen atoms were located and then fixed at O-H = 0.85 Å and with $U_{\text{iso}}=1.5U_{\text{eq}}(\text{O})$.

For compound **2**, significant residual electron density peak near Mo atom ($> 3.5 \text{ e A}^{-3}$) indicated unequal disorder of the coordinated molybdate anion. It was possible to resolve such the disordering scheme with refined occupancy factors of 0.946 and 0.054. The oxygen atom O1 and O2 are common for two contributions and they were refined with occupancies of 1.0. To improve the refinement stability, a soft SADI restraint was applied for each pair of chemically equivalent bonds of two disordered MoO_2 fragments. Considering very small contribution from the minor component of the disorder, the corresponding atoms were left isotropic. One solvate water molecule overlaps with the minor contribution of the MoO_4 disorder. Water molecule referenced by the oxygen atom O3W is disordered over inversion centre and another solvent molecule is equally disorder over two closely separated positions (O41W and O42W). The latter oxygen atom was refined isotropically.

For compound **3**, the assignment of O/F ligand atoms was evident by refinement of thermal parameters and by analysis of the crystal structure environment, such as H-bonding patterns.

Crystallographic positions of F atoms on one of two centrosymmetric $[\text{Mo}_8\text{O}_{26}\text{F}_2]^{6-}$ units were refined utilizing a F/O disorder scheme, using EADP and EXYZ, with equal occupancy factors (0.5). Oxygen atoms of water molecules (O1, O4w), which do not show two characteristic contacts clearly associated with H-bonding, were refined anisotropically without protons.

Table S1. Crystal data for complexes **1-3**.

	1	2	3
Formula	C ₇ H ₁₀ F ₂ Mo ₂ N ₆ O ₅	C ₁₄ H ₃₄ Co ₃ F ₂ Mo ₂ N ₁₂ O ₁₅	C ₂₁ H ₄₀ Co ₃ F ₂ Mo ₈ N ₁₈ O ₃₁
T / K	296	296	296
M	488.09	1017.20	2023.02
Crystal system	Orthorhombic	Triclinic	Triclinic
Space group, Z	Pmmn, 2	P $\bar{1}$, 1	P $\bar{1}$, 2
a / Å	10.7334(11)	8.8925(6)	12.6171(2)
b / Å	11.8312(11)	9.3345(6)	13.5719(3)
c / Å	5.5037(6)	10.8401(8)	14.8734(3)
$\alpha/^\circ$	90	65.197(5)	96.9040(10)
$\beta/^\circ$	90	86.104(5)	94.8820(10)
$\gamma/^\circ$	90	73.474(5)	94.1450(10)
V / Å ³	698.91(12)	781.70(9)	2510.47(9)
$\mu(\text{Mo-K}\alpha) / \text{mm}^{-1}$	1.851	2.435	3.008
D _c / g cm ⁻³	2.319	2.161	2.676
$\theta_{\max} (\circ)$	27.03	27.48	30.45
Meas / Unique reflns	3714 / 837	13896 / 3571	40824 / 14950
Parameters refined	60	235	751
R ₁ , wR ₂	0.030, 0.055	0.055, 0.097	0.030, 0.067
[I > 2σ(I)]			
R ₁ , wR ₂	0.039, 0.058	0.104, 0.110	0.038, 0.069
(all data)			
Goof on F^2	1.030	0.992	1.063
Max, min / peak e Å ⁻³	0.57, -1.10	0.832, -1.01	1.39, -1.71

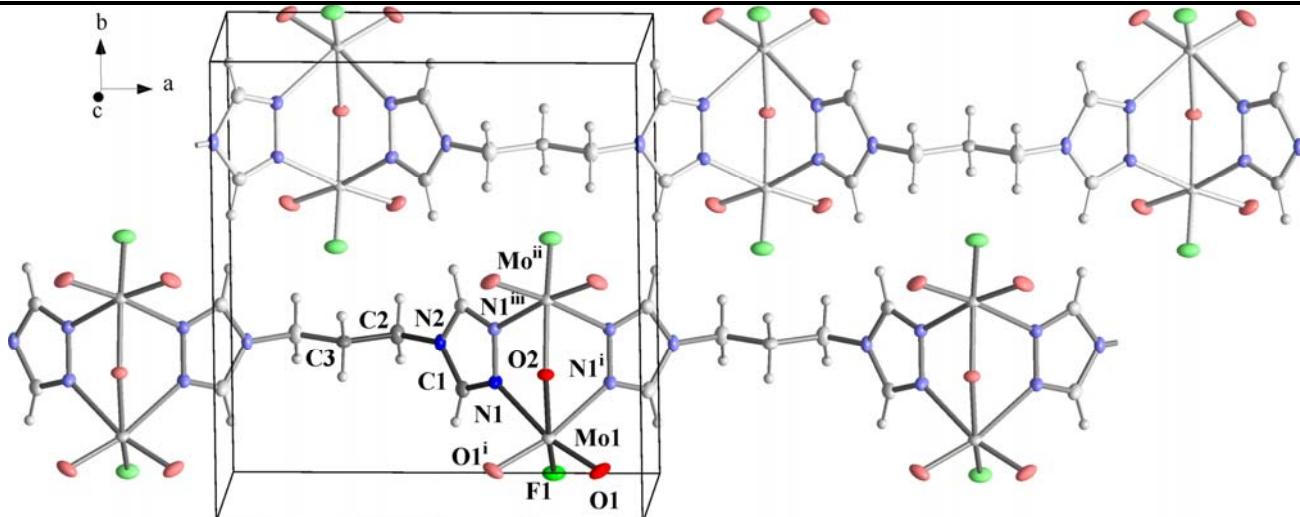


Figure S1. Crystal structure and labeling scheme for $[Mo_2F_2O_5(tr_2pr)]$, (1). Ellipsoids are shown at the 50% probability level.

Table S2. Selected bond lengths (\AA) and angles ($^\circ$) for 1.

$[Mo_2F_2O_5(tr_2pr)]$, (1), symmetry codes: (i) $-x+3/2, y, z$; (ii) $-x+3/2, -y+1/2, z$; (iii) $x, -y+1/2, z$.			
Mo(1)—O(1)	1.696 (3)	O(1)i—Mo(1)—O(1)	104.85 (19)
Mo(1)—O(2)	1.9030 (16)	O(1)—Mo(1)—O(2)	101.21 (12)
Mo(1)—F(1)	1.917 (3)	O(1)—Mo(1)—F(1)	96.90 (10)
Mo(1)—N(1)	2.343 (3)	O(2)—Mo(1)—F(1)	150.04 (16)
N(1)—C(1)	1.298 (4)	O(1)—Mo(1)—N(1)i	89.53 (12)
N(1)—N(1)iii	1.385 (6)	O(2)—Mo(1)—N(1)	77.26 (12)
N(2)—C(1)	1.353 (4)	N(1)i—Mo(1)—N(1)	76.04 (14)
N(2)—C(2)	1.470 (6)	O(1)—Mo(1)—N(1)	165.50 (12)
		F(1)—Mo(1)—N(1)	79.25 (10)
		Mo(1)—O(2)—Mo(1)ii	139.8 (3)
		C(1)—N(1)—N(1)iii	107.2 (2)
		C(1)—N(1)—Mo(1)	134.9 (2)
		N(1)iii—N(1)—Mo(1)	117.85 (7)

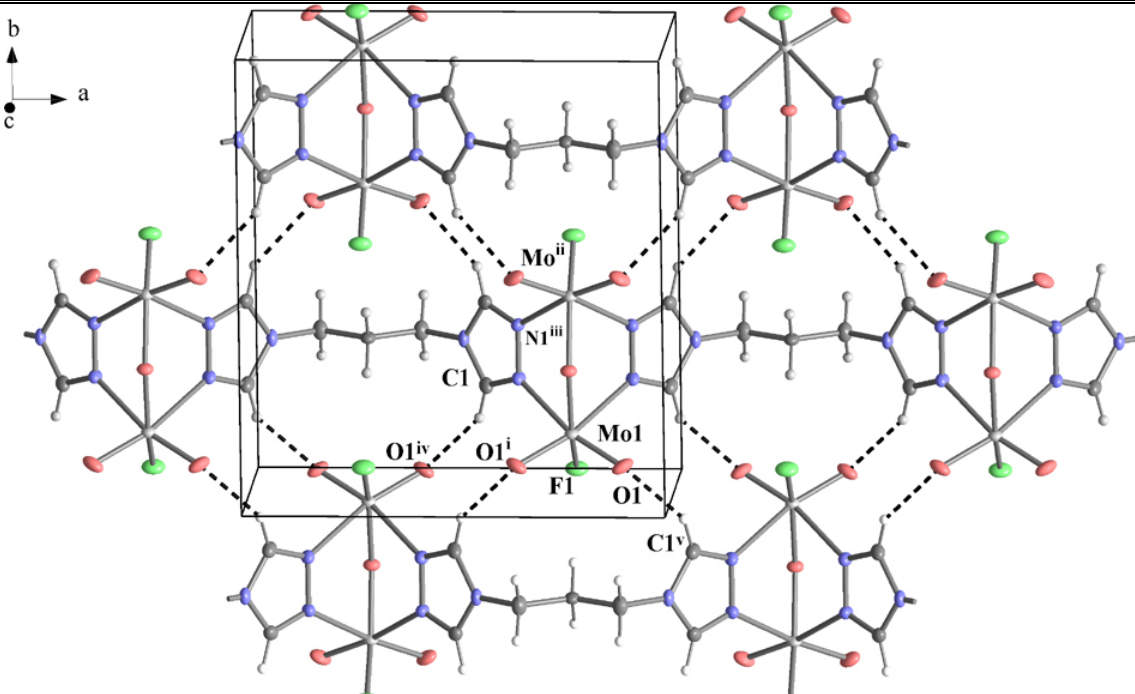


Figure S2. Illustration of a 2D H-bonding pattern in the crystal structure of $[\text{Mo}_2\text{F}_2\text{O}_5(\text{tr}_2\text{pr})]$, **(1)**. (Symmetry codes: (i) $-x+3/2, y, z$; (ii) $-x+3/2, -y+1/2, z$; (iii) $x, -y+1/2, z$; (iv) $-1/2+x, -y, -z$; (v) $1/2+x, -y, -z$. $\text{C}1\text{-H}1\dots\text{O}1(\text{iv})$ 3.071 (4), $\angle\text{C}1\text{-H}1\dots\text{O}1(\text{iv})$ 149.00°.

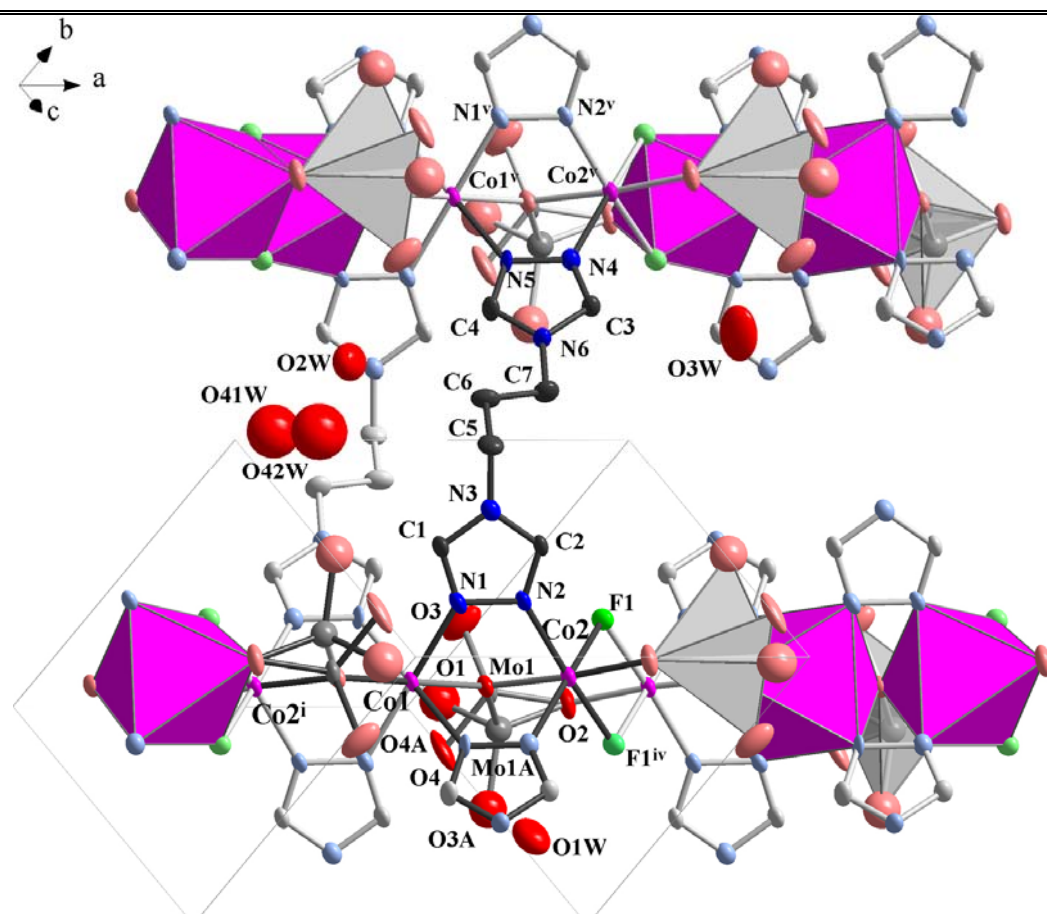


Figure S3. Crystal structure and labeling scheme for $[\text{Co}_3(\text{tr}_2\text{pr})_2(\text{MoO}_4)_2\text{F}_2]\cdot7\text{H}_2\text{O}$ **(2)**; (i) $-x+1, -y+1, -z+1$; (ii) $x, y-1, z+1$; (iii) $-x+1, -y+2, -z$; (iv) $-x+2, -y+1, -z+1$; (v) $x, y+1, z-1$.

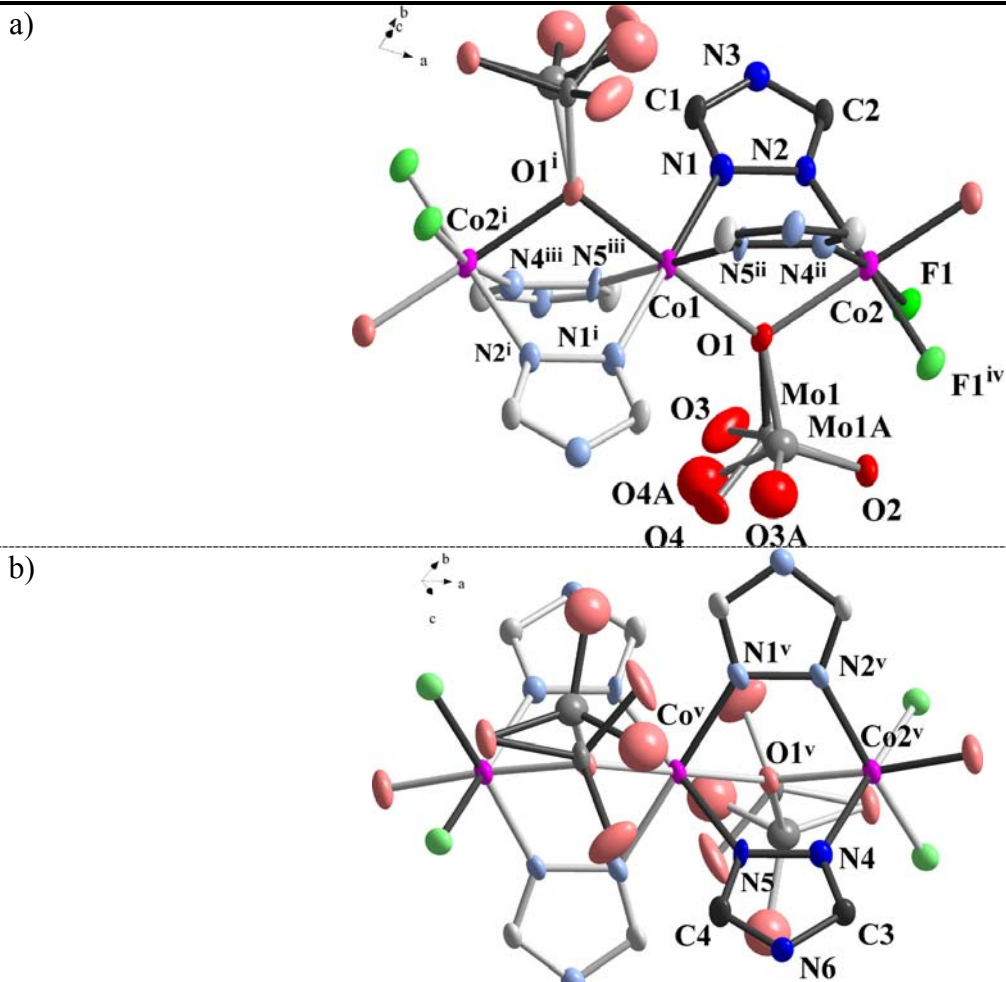


Figure S4. Illustration of the centrosymmetrical trinuclear fragments in the crystal structure **2**. (i) -x+1, -y+1, -z+1; (ii) x, y-1, z+1; (iii) -x+1, -y+2, -z; (iv) -x+2, -y+1, -z+1; (v) x, y+1, z-1.

Table S3. Selected bond lengths (\AA) and angles ($^\circ$) for **2**.

[$\text{[Co}_3(\text{tr}_{2}\text{pr})_2(\text{MoO}_4)_2\text{F}_2]\cdot 7\text{H}_2\text{O}$ (**2**)], symmetry codes: (i) -x+1, -y+1, -z+1; (ii) x, y-1, z+1; (iii) -x+1, -y+2, -z; (iv) -x+2, -y+1, -z+1; (v) x, y+1, z-1.

F(1)—Co(2)	2.057(3)	Co(2)—O(1)	2.159(4)
Co(1)—O(1)i	2.104(4)	O(1)—Mo(1A)	1.823(8)
Co(1)—O(1)	2.104(4)	O(1)—Mo(1)	1.833(4)
Co(1)—N(1)i	2.122(5)	O(2)—Mo(1)	1.758(4)
Co(1)—N(5)ii	2.123(5)	O(2)—Mo(1A)	1.772(8)
Co(1)—N(5)iii	2.123(5)	Mo(1)—O(4)	1.722(5)
Co(2)—F(1)iv	2.041(3)	Mo(1)—O(3)	1.727(5)
Co(2)—O(2)iv	2.054(4)	Mo(1A)—O(4A)	1.723(9)
Co(2)—N(4)ii	2.105(5)	Mo(1A)—O(3A)	1.726(10)

Table S3. continued.

Co(2)iv—F(1)—Co(2)	97.07(14)	F(1)—Co(2)—Co(2)iv	41.26(9)
O(1)i—Co(1)—N(1)	93.76(16)	N(2)—Co(2)—Co(2)iv	132.03(13)
O(1)—Co(1)—N(1)	86.24(16)	N(4)ii—Co(2)—Co(2)iv	132.37(13)
O(1)i—Co(1)—N(5)ii	94.24(16)	O(1)—Co(2)—Co(2)iv	88.99(10)
O(1)—Co(1)—N(5)ii	85.76(16)	F(1)iv—Co(2)—Co(1)	118.62(9)
N(1)—Co(1)—N(5)ii	93.30(18)	O(2)iv—Co(2)—Co(1)	145.18(11)
N(1)i—Co(1)—N(5)ii	86.70(18)	F(1)—Co(2)—Co(1)	114.27(9)
O(1)i—Co(1)—Co(2)	141.42(10)	N(2)—Co(2)—Co(1)	62.81(12)
O(1)—Co(1)—Co(2)	38.58(10)	N(4)ii—Co(2)—Co(1)	63.26(13)
N(1)—Co(1)—Co(2)	61.63(13)	O(1)—Co(2)—Co(1)	37.43(9)
N(1)i—Co(1)—Co(2)	118.37(13)	Co(2)iv—Co(2)—Co(1)	126.42(4)
N(5)ii—Co(1)—Co(2)	60.95(12)	Mo(1A)—O(1)—Co(1)	134.3(3)
N(5)iii—Co(1)—Co(2)	119.05(12)	Mo(1)—O(1)—Co(1)	134.31(19)
F(1)iv—Co(2)—O(2)iv	89.11(14)	Mo(1A)—O(1)—Co(2)	113.5(4)
F(1)iv—Co(2)—F(1)	82.93(14)	Mo(1)—O(1)—Co(2)	121.58(18)
O(2)iv—Co(2)—F(1)	88.11(15)	Co(1)—O(1)—Co(2)	103.99(15)
F(1)iv—Co(2)—N(2)	173.56(16)	Mo(1)—O(2)—Co(2)iv	127.3(2)
O(2)iv—Co(2)—N(2)	92.10(17)	Mo(1A)—O(2)—Co(2)iv	120.7(4)
F(1)—Co(2)—N(2)	90.79(15)	O(4)—Mo(1)—O(3)	106.1(3)
F(1)iv—Co(2)—N(4)ii	91.01(15)	O(4)—Mo(1)—O(2)	109.2(2)
O(2)iv—Co(2)—N(4)ii	98.17(17)	O(3)—Mo(1)—O(2)	108.7(2)
F(1)—Co(2)—N(4)ii	171.23(15)	O(4)—Mo(1)—O(1)	111.0(2)
N(2)—Co(2)—N(4)ii	95.07(18)	O(3)—Mo(1)—O(1)	109.9(2)
F(1)iv—Co(2)—O(1)	91.79(13)	O(2)—Mo(1)—O(1)	111.74(17)
O(2)iv—Co(2)—O(1)	174.60(16)	O(4A)—Mo(1A)—O(3A)	106.1(7)
F(1)—Co(2)—O(1)	86.72(14)	O(4A)—Mo(1A)—O(2)	103(4)
N(2)—Co(2)—O(1)	86.43(16)	O(3A)—Mo(1A)—O(2)	116(4)
N(4)ii—Co(2)—O(1)	87.14(16)	O(4A)—Mo(1A)—O(1)	102(4)
F(1)iv—Co(2)—Co(2)iv	41.68(9)	O(3A)—Mo(1A)—O(1)	117(4)
O(2)iv—Co(2)—Co(2)iv	8.14(11)	O(2)—Mo(1A)—O(1)	111.6(5)

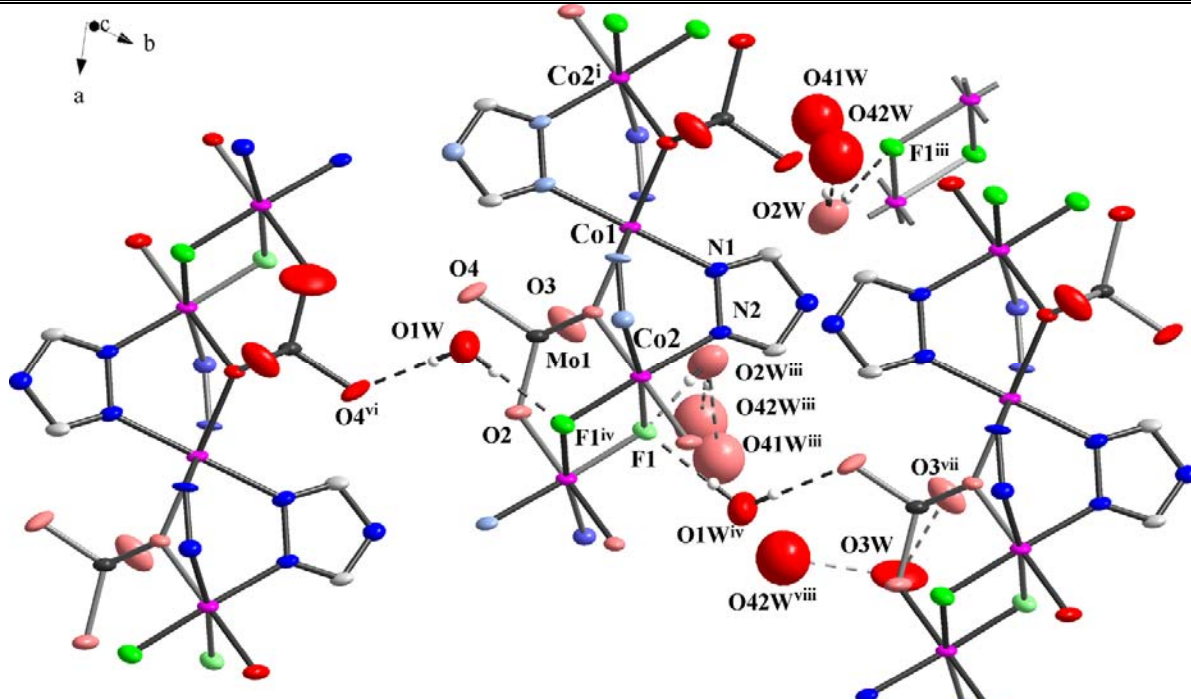


Figure S5. The H-bonding patterns showing the interconnections between the neighboring $[Co_3(tr)_4(MoO_4)_2F_2]_n$ chains; symmetry codes: (i) $-x+1, -y+1, -z+1$; (ii) $x, y-1, z+1$; (iii) $-x+1, -y+2, -z$; (iv) $-x+2, -y+1, -z+1$; (v) $x, y+1, z-1$; (vi) $-x+2, -y, -z+1$; (vii) $x, 1+y, z$; (viii) $1+x, y, z..$

Table S4. Hydrogen bonding scheme in the crystal structure of **2** (\AA , $^\circ$).

$D\cdots H\cdots A$	$H\cdots A$	$D\cdots A$	$D\cdots H\cdots A$
O(1W)iv-H(1W)iv...F(1)	1.90	2.752(7)	176
O(1W)-H(2W)...O(4)vi	2.06	2.912(8)	176
O(2W)-H(3W)...F(1)iii	2.05	2.900(7)	176
O(2W)-H(4W)...O(41W)	1.95	2.76(2)	160
O(2W)-H(4W)...O(42W)	1.91	2.74(2)	166
C(1)-H(1)...O(1W)i	2.40	3.307(9)	166
C(2)-H(2)...O(4)vii	2.17	3.063(8)	160
C(3)-H(3)...O(3W)	2.38	3.301(16)	172
C(4)-H(4)...O(2W)	2.33	3.229(9)	162
C(7)-H(7A)...O(3)vii	2.57	3.522(9)	167
C(7)-H(7B)...O(2W)iii	2.48	3.353(10)	150

-x+1, -y+1, -z+1; (ii) x, y-1, z+1; (iii) -x+1, -y+2, -z; (iv) -x+2, -y+1, -z+1; (v) x, y+1, z-1; (vi) -x+2, -y, -z+1; (vii) x, 1+y, z; (viii) 1+x, y, z..

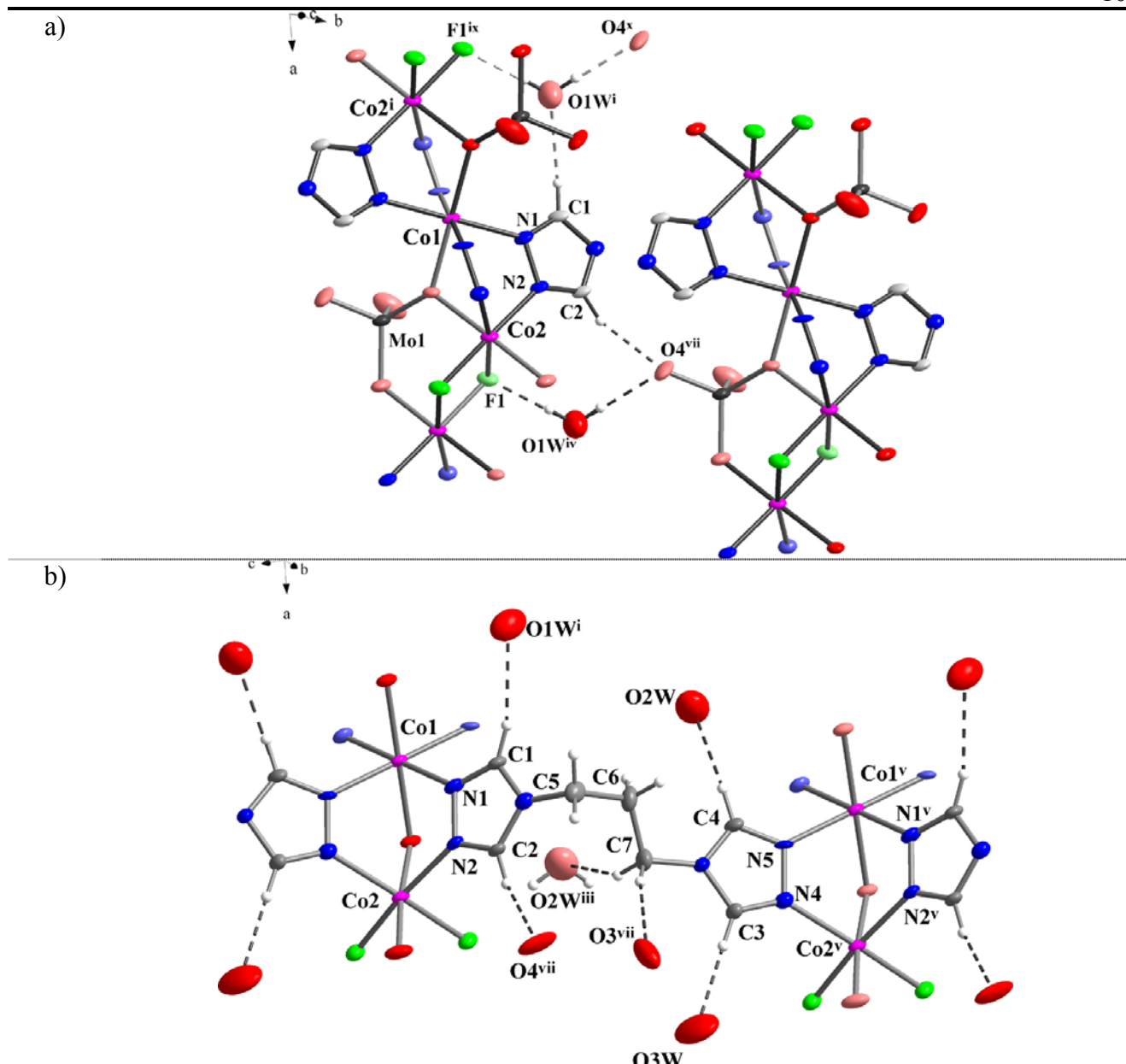


Figure S6. Illustration of the C-H...O and O-H...O(or F) contacts in the crystal structure **2**; symmetry codes: (i) $-x+1, -y+1, -z+1$; (ii) $x, y-1, z+1$; (iii) $-x+1, -y+2, -z$; (iv) $-x+2, -y+1, -z+1$; (v) $x, y+1, z-1$; (vi) $-x+2, -y, -z+1$; (vii) $x, 1+y, z$; (viii) $1+x, y, z$; (ix) $-1+x, y, z$; (x) $-1+x, 1+y, z$.

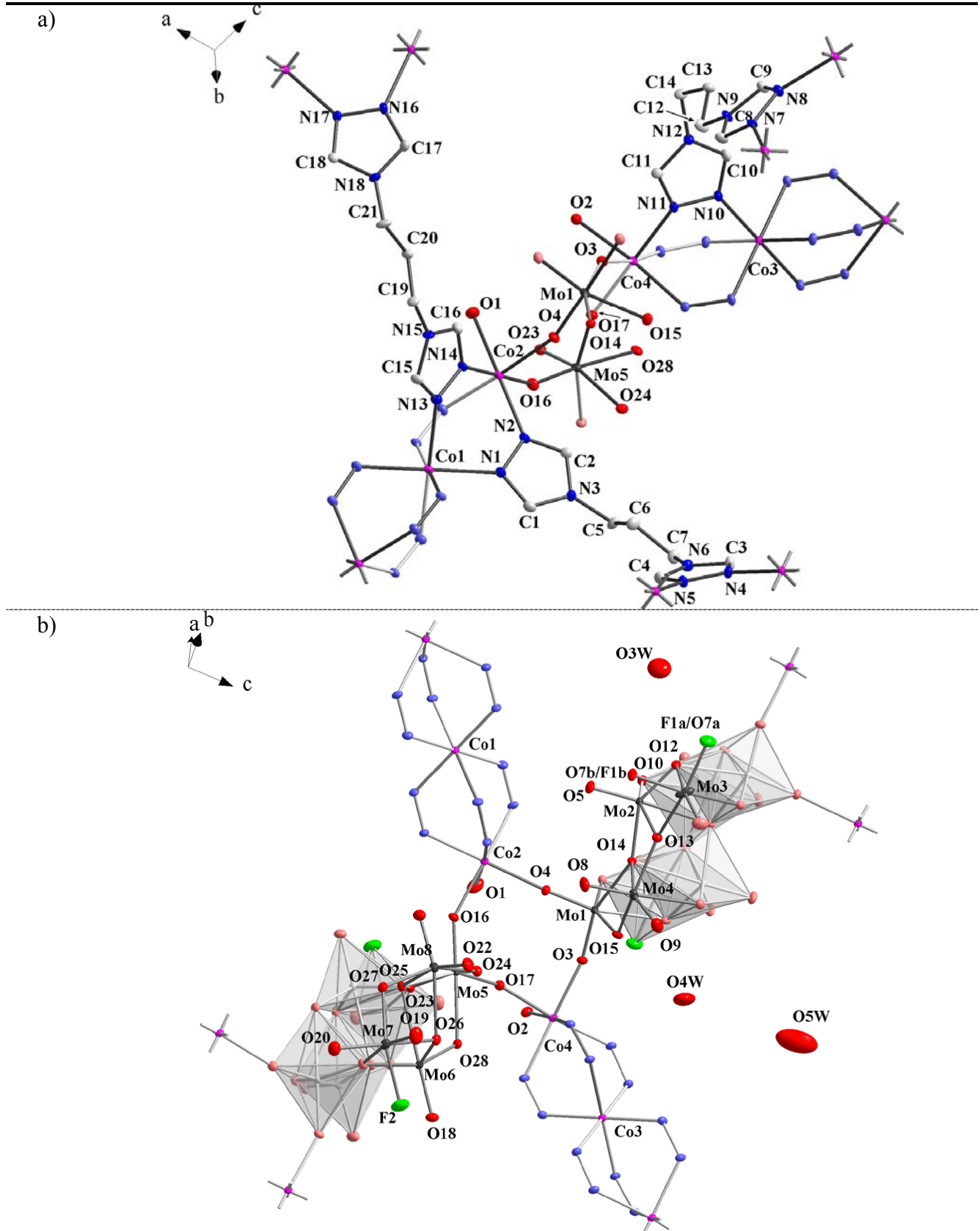


Figure S7. Crystal structure and labeling scheme for $[\text{Co}_3(\text{H}_2\text{O})_2(\text{tr}_2\text{pr})_3(\text{Mo}_8\text{O}_{26}\text{F}_2)] \cdot 3\text{H}_2\text{O}$ (**3**). Ellipsoids are shown at the 50% probability level.

Table S5. Selected bond lengths (\AA) and angles ($^\circ$) for **3**.

$[\text{Co}_3(\text{H}_2\text{O})_2(\text{tr}_{2\text{pr}})_3(\text{Mo}_8\text{O}_{26}\text{F}_2)] \cdot 3\text{H}_2\text{O}$ (3), symmetry codes: (i) $-x+1, -y+1, -z+1$; (ii) $x, y, z-1$; (iii) $-x+1, -y+1, -z$; (iv) $-x, -y+1, -z+1$; (v) $x, y-1, z$; (vi) $-x, -y, -z+1$; (vii) $-x+1, -y, -z+1$; (viii) $x-1, y, z$; (ix) $-x, -y, -z$; (x) $x, y+1, z$; (xi) $x, y, z+1$; (xii) $x+1, y, z$.			
Co1—N7i	2 x 2.107 (3)	Co3—N4iv	2 x 2.118 (3)
Co1—N1	2 x 2.150 (3)	Co3—N10	2 x 2.120 (3)
Co1—N13	2 x 2.167 (3)	Co3—N16vii	2 x 2.153 (3)
Co2—N2	2.068 (3)	Co4—N5v	2.092 (3)
Co2—N14	2.076 (3)	Co4—N11	2.097 (3)
Co2—N8ii	2.098 (3)	Co4—N17vii	2.076 (3)
Co2—O1	2.161 (3)	Co4—O3	2.055 (2)
Co2—O16	2.098 (2)	Co4—O17	2.061 (2)
Co2—O4	2.131 (2)	Co4—O2	2.154 (2)
Co1—Co2	3.8236 (4)	Co3—Co4	3.8028 (4)
N7i—Co1—N7ii	180.00	O17—Co4—N5v	95.31 (10)
N7i—Co1—N1	90.15 (10)	N17vii—Co4—N5v	90.41 (11)
N7i—Co1—N13iii	87.65 (10)	O3—Co4—N11	86.43 (10)
N1iii—Co1—N13iii	89.84 (10)	O17—Co4—N11	174.31 (10)
N7i—Co1—Co2	125.70 (7)	N17vii—Co4—N11	90.14 (11)
N7ii—Co1—Co2	54.30 (7)	N5v—Co4—N11	90.22 (11)
N1—Co1—Co2	54.23 (7)	O3—Co4—O2	86.61 (9)
N2—Co2—N14	92.23 (11)	O17—Co4—O2	85.00 (9)
N2—Co2—O16	88.93 (10)	N17vii—Co4—O2	172.36 (10)
N14—Co2—O16	177.82 (10)	N5v—Co4—O2	86.23 (10)
N2—Co2—N8ii	89.24 (11)	N11—Co4—O2	96.72 (10)
N14—Co2—N8ii	90.45 (11)	O3—Co4—Co3	127.62 (7)
O16—Co2—N8ii	87.71 (10)	O17—Co4—Co3	128.98 (6)
N8—N7—Co1xi	125.7 (2)	N17vii—Co4—Co3	56.09 (8)
N14—N13—Co1	124.8 (2)	N10—N11—Co4	128.2 (2)
Mo1—O4—Co2	160.54 (14)	N11—N10—Co3	121.5 (2)
O2—Co4—Co3	126.14 (6)	Mo1—O3—Co4	147.66 (13)
N11—Co4—Co3	53.89 (7)	N5v—Co4—Co3	54.79 (7)

Table S5. continued.

Mo1—O4	1.736 (2)	Mo5—O17	1.735 (2)
Mo1—O3	1.736 (2)	Mo5—O16	1.735 (2)
Mo1—O11i	1.836 (2)	Mo5—O23	1.893 (2)
Mo1—O15	1.991 (2)	Mo5—O24	1.910 (2)
Mo1—O14	2.189 (2)	Mo5—O25	2.180 (2)
Mo1—O12i	2.355 (2)	Mo5—O28	2.308 (2)
Mo2—O5	1.697 (2)	Mo6—O18	1.704 (2)
Mo2—O10	1.749 (2)	Mo6—O28	1.744 (2)
Mo2—O12	1.875 (2)	Mo6—O26	1.890 (2)
Mo2—O14	1.946 (2)	Mo6—O25ix	1.953 (2)
Mo2—O13	2.200 (2)	Mo6—O23ix	2.133 (2)
Mo2—O14i	2.451 (2)	Mo6—O25	2.537 (2)
Mo3—O6	1.697 (2)	Mo7—O19	1.703 (3)
Mo3—F1B	1.822 (2)	Mo7—O20	1.721 (3)
Mo3—O7A	1.828 (2)	Mo7—O27	1.903 (2)
Mo3—O13	2.010 (2)	Mo7—F2	1.977 (2)
Mo3—O11	2.080 (2)	Mo7—O23ix	2.189 (2)
Mo3—O12	2.201 (2)	Mo7—O26	2.206 (2)
Mo4—O8	1.701 (2)	Mo8—O22	1.710 (2)
Mo4—O9	1.729 (2)	Mo8—O21	1.716 (2)
Mo4—O15	1.891 (2)	Mo8—O27	1.939 (2)
Mo4—O13	1.955 (2)	Mo8—O24	1.953 (2)
Mo4—O14	2.241 (2)	Mo8—O25	2.262 (2)
Mo4—O10i	2.364 (2)	Mo8—O26	2.285 (2)
<hr/>			
O27—Mo8—O24	151.47 (10)	Mo5—O16—Co2	148.28 (14)
O22—Mo8—O25	163.50 (11)	Mo5—O17—Co4	158.97 (13)
O21—Mo8—O25	91.28 (10)	Mo5—O23—Mo6ix	107.19 (10)
O27—Mo8—O25	85.08 (9)	Mo5—O23—Mo7ix	149.82 (13)
O24—Mo8—O25	71.68 (9)	Mo6ix—O23—Mo7ix	102.97 (10)
<hr/>			

Table S5. continued.

O22—Mo8—O26	91.92 (10)	Mo5—O24—Mo8	115.65 (12)
O21—Mo8—O26	163.81 (11)	Mo6ix—O25—Mo5	103.27 (9)
O27—Mo8—O26	72.99 (9)	Mo6ix—O25—Mo8	153.08 (12)
O24—Mo8—O26	84.81 (9)	Mo5—O25—Mo8	94.82 (9)
O25—Mo8—O26	74.74 (8)	Mo6ix—O25—Mo6	103.72 (9)
Mo2—O10—Mo4i	114.87 (11)	Mo5—O25—Mo6	95.30 (8)
Mo1i—O11—Mo3	116.54 (11)	Mo8—O25—Mo6	94.13 (8)
Mo2—O12—Mo3	106.43 (10)	Mo6—O26—Mo7	111.08 (11)
Mo2—O12—Mo1i	112.82 (11)	Mo6—O26—Mo8	114.48 (10)
Mo3—O12—Mo1i	93.99 (8)	Mo7—O26—Mo8	91.94 (9)
Mo4—O13—Mo3	151.54 (12)	Mo7—O27—Mo8	114.38 (12)
Mo4—O13—Mo2	106.11 (10)	Mo6—O28—Mo5	118.49 (11)
Mo3—O13—Mo2	101.82 (10)	O8—Mo4—O14	102.78 (10)
Mo2—O14—Mo1	147.64 (11)	O9—Mo4—O14	153.90 (11)
Mo2—O14—Mo4	104.90 (9)	O15—Mo4—O14	72.16 (9)
Mo1—O14—Mo4	95.39 (8)	O13—Mo4—O14	71.84 (9)
Mo2—O14—Mo2i	103.65 (9)	O8—Mo4—O10i	174.20 (10)
O4—Mo1—O3	103.47 (11)	O9—Mo4—O10i	82.44 (10)
O4—Mo1—O11i	100.90 (10)	O15—Mo4—O10i	80.78 (9)
O3—Mo1—O11i	102.20 (10)	O13—Mo4—O10i	80.58 (9)
O4—Mo1—O15	101.85 (10)	O14—Mo4—O10i	71.46 (8)
O3—Mo1—O15	91.01 (10)	O17—Mo5—O16	101.52 (11)
O11i—Mo1—O15	150.15 (10)	O17—Mo5—O23	102.15 (10)
O4—Mo1—O14	94.89 (10)	O16—Mo5—O23	98.79 (10)
O3—Mo1—O14	157.03 (10)	O17—Mo5—O24	103.73 (10)
O11i—Mo1—O14	87.50 (9)	O16—Mo5—O24	96.47 (10)
O15—Mo1—O14	71.56 (9)	O23—Mo5—O24	146.53 (10)
O4—Mo1—O12i	166.15 (10)	O17—Mo5—O25	153.80 (10)
O3—Mo1—O12i	90.23 (10)	O16—Mo5—O25	104.66 (10)
O11i—Mo1—O12i	73.79 (9)	O23—Mo5—O25	73.05 (9)

Table S5. continued.

O15—Mo1—O12i	79.59 (9)	O24—Mo5—O25	74.34 (9)
O14—Mo1—O12i	72.34 (8)	O17—Mo5—O28	81.65 (9)
O5—Mo2—O10	104.21 (11)	O16—Mo5—O28	175.61 (10)
O5—Mo2—O12	104.97 (11)	O23—Mo5—O28	83.40 (9)
O10—Mo2—O12	101.37 (10)	O24—Mo5—O28	79.76 (9)
O5—Mo2—O14	102.30 (11)	O25—Mo5—O28	72.25 (8)
O10—Mo2—O14	99.16 (10)	O18—Mo6—O28	104.18 (11)
O12—Mo2—O14	140.36 (9)	O18—Mo6—O26	105.55 (11)
O5—Mo2—O13	96.64 (10)	O28—Mo6—O26	100.74 (10)
O10—Mo2—O13	158.91 (10)	O18—Mo6—O25ix	103.56 (11)
O12—Mo2—O13	75.82 (9)	O28—Mo6—O25ix	97.53 (10)
O14—Mo2—O13	72.91 (9)	O26—Mo6—O25ix	140.38 (10)
O5—Mo2—O14i	177.87 (10)	O18—Mo6—O23ix	99.92 (11)
O10—Mo2—O14i	77.69 (9)	O28—Mo6—O23ix	155.61 (10)
O12—Mo2—O14i	75.43 (9)	O26—Mo6—O23ix	75.97 (9)
O14—Mo2—O14i	76.35 (9)	O25ix—Mo6—O23ix	73.00 (9)
O13—Mo2—O14i	81.41 (8)	O18—Mo6—O25	177.91 (10)
O6—Mo3—F1B	102.33 (11)	O28—Mo6—O25	73.81 (9)
O6—Mo3—O7A	101.88 (12)	O26—Mo6—O25	75.56 (8)
F1B—Mo3—O7A	90.88 (11)	O25ix—Mo6—O25	76.28 (9)
O6—Mo3—O13	98.57 (11)	O23ix—Mo6—O25	82.04 (8)
F1B—Mo3—O13	158.46 (9)	O19—Mo7—O20	105.22 (13)
O7A—Mo3—O13	89.88 (10)	O19—Mo7—O27	97.89 (12)
O6—Mo3—O11	92.47 (11)	O20—Mo7—O27	98.42 (11)
F1B—Mo3—O11	87.50 (10)	O19—Mo7—F2	90.29 (12)
O7A—Mo3—O11	165.58 (10)	O20—Mo7—F2	97.72 (11)
O13—Mo3—O11	86.44 (9)	O27—Mo7—F2	159.28 (10)
O6—Mo3—O12	163.53 (11)	O19—Mo7—O23ix	163.83 (11)
F1B—Mo3—O12	85.20 (9)	O20—Mo7—O23ix	88.85 (11)
O7A—Mo3—O12	92.53 (10)	O27—Mo7—O23ix	87.66 (9)

Table S5. continued.

O13—Mo3—O12	73.26 (9)	F2—Mo7—O23ix	79.76 (9)
O11—Mo3—O12	73.05 (9)	O19—Mo7—O26	97.76 (11)
O8—Mo4—O9	103.32 (12)	O20—Mo7—O26	156.88 (10)
O8—Mo4—O15	98.23 (11)	O27—Mo7—O26	75.53 (9)
O9—Mo4—O15	103.79 (11)	F2—Mo7—O26	84.55 (9)
O8—Mo4—O13	97.17 (11)	O23ix—Mo7—O26	68.82 (8)
O9—Mo4—O13	104.92 (11)	O22—Mo8—O21	103.15 (13)
O15—Mo4—O13	143.13 (9)	O22—Mo8—O27	100.50 (11)
Mo1—O14—Mo2i	99.02 (8)	O21—Mo8—O27	98.12 (11)
Mo4—O14—Mo2i	95.70 (8)	O22—Mo8—O24	97.89 (11)
Mo4—O15—Mo1	115.11 (11)	O21—Mo8—O24	98.70 (11)

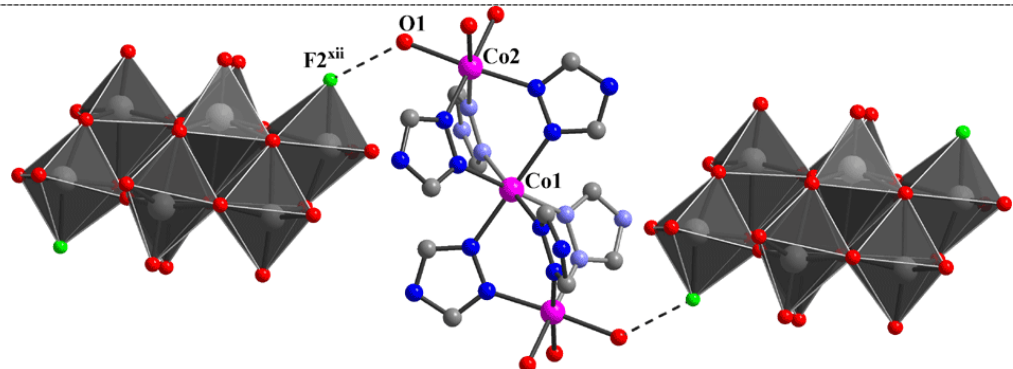


Figure S8. The O-H...F hydrogen-bonding interactions between coordinating water and $[\text{Mo}_8\text{O}_{26}\text{F}_2]^{6-}$ -anions ($\text{O}1\text{-H}...\text{F}2 = 2.843(4)$ Å) in the crystal structure of **3**; symmetry code: (xii) $x+1, y, z$;

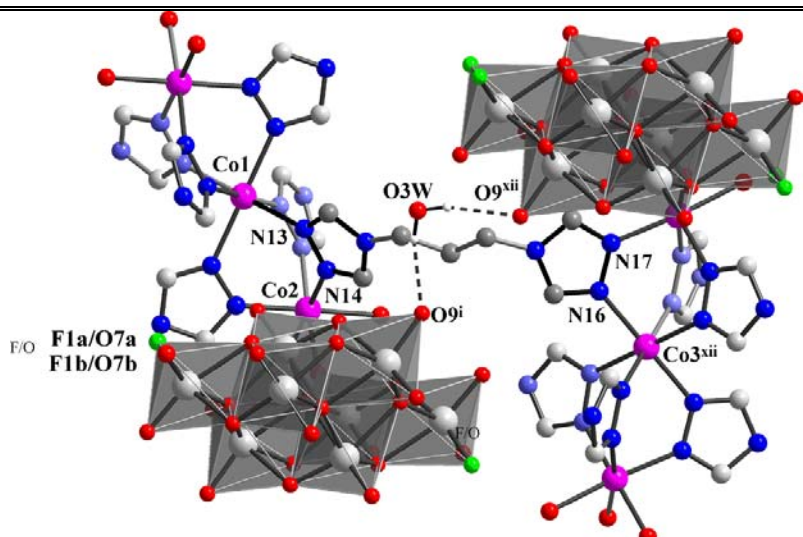


Figure S9. Hydrogen-bonding interactions between non-coordinating water molecule and $[\text{Mo}_8\text{O}_{26}\text{F}_2]^{6-}$ -anions in the crystal structure of **3**; symmetry codes: (i) $-x+1, -y+1, -z+1$; (xii) $x+1, y, z$;

Table S6. Hydrogen bonding scheme in the crystal structure of **3** (Å, °).

N	D-H···A	H···A	D···A	D-H···A
1.	O(3W)—H(3WB)...O(9)i	2.17	3.000(5)	166
2.	O(3W)—H(3WA)...O(9)xii	2.10	2.930(5)	166
3.	O(2)—H(2A)...F(1A)/O(7A)v	2.00	2.799(3)	157
4.	O(2)—H(2B)...O(20)ix	1.96	2.805(4)	170
5.	O(5W)—H(5WA)...O(21)xi	2.07	2.901(5)	164
6.	O(5W)—H(5WB)...O(18)vi	2.18	3.004(5)	164
7.	C(1)—H(1)...O(19)xiii	2.40	3.319(5)	168
8.	C(2)—H(2)...O(24)	2.56	3.370(4)	146
9.	C(3)—H(3)...O(4W)iv	2.24	3.139(5)	162
10.	C(4)—H(4)...O(27)xiii	2.51	3.216(4)	133
11.	C(5)—H(5B)...O(21)xiii	2.58	3.438(5)	147
12.	C(6)—H(6A)...O(8)	2.49	3.316(5)	143
13.	C(7)—H(7A)...O(21)xiii	2.26	3.203(4)	164
14.	C(8)—H(8)...O(5)i	2.11	3.020(4)	167
15.	C(11)—H(11)...F1B/O(7B)i	2.15	3.046(4)	162
16.	C(13)—H(13B)...O(18)vi	2.44	3.351(4)	156
17.	C(14)—H(14A)...O(2)	2.45	3.283(4)	144
18.	C(15)—H(15)...O(5W)i	2.39	3.250(6)	154
19.	C(16)—H(16)...O(11)i	2.31	3.140(4)	148
20.	C(17)—H(17)...O(6)i	2.17	3.056(4)	159
21.	C(19)—H(19A)...O(9)i	2.55	3.365(4)	141
22.	C(19)—H(19A)...O(10)	2.43	3.173(4)	133
23.	C(21)—H(21B)...O(9)i	2.54	3.357(5)	142

(i)1-x, 1-y, 1-z, (iv) -x, -y+1, -z+1; (v) x, y-1, z; (vi) -x, -y, -z+1; (ix) -x, -y, -z; (xi) x, y, z+1;
 (xii) x+1, y, z; (xiii) -x, 1-y, -z

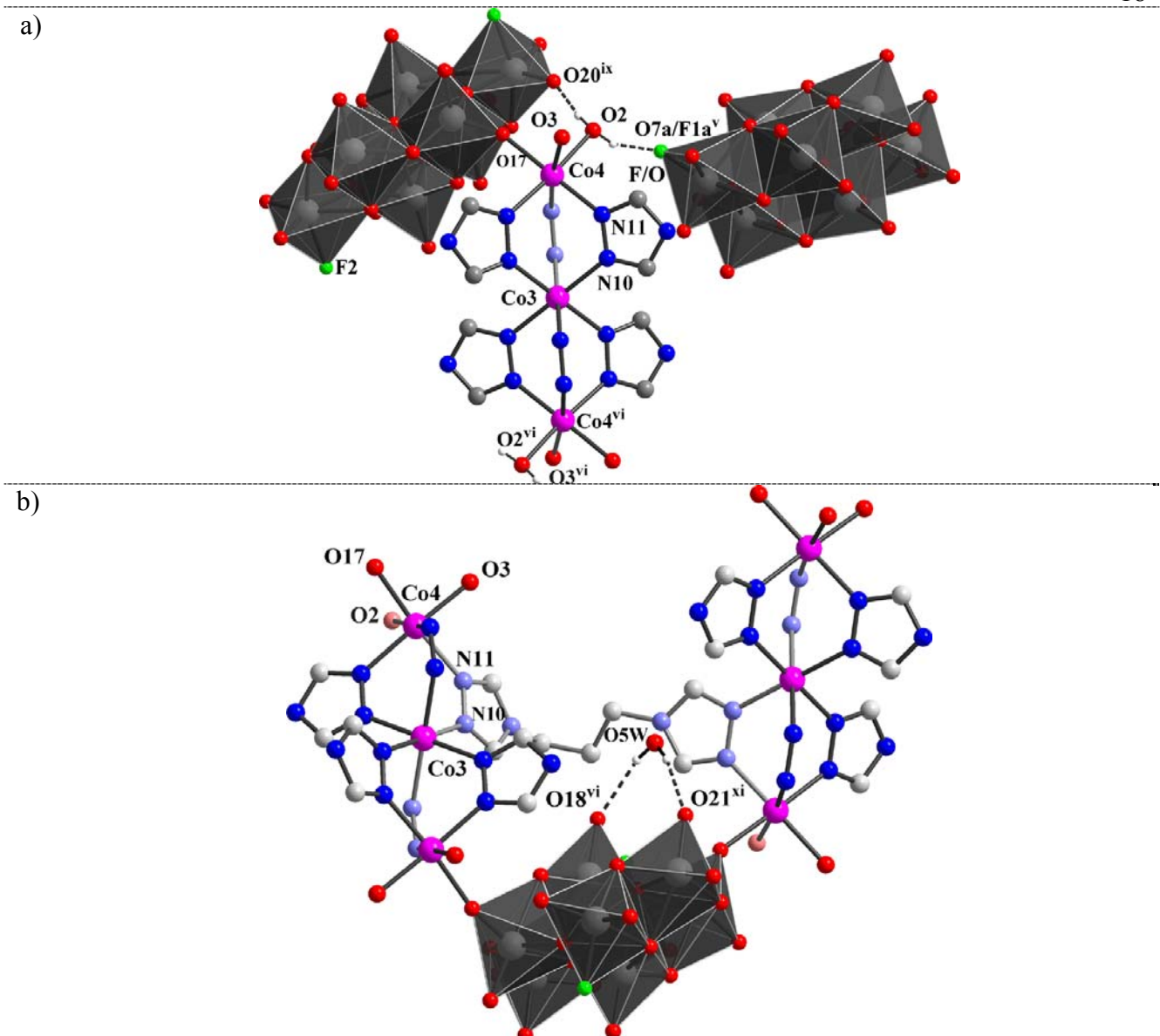
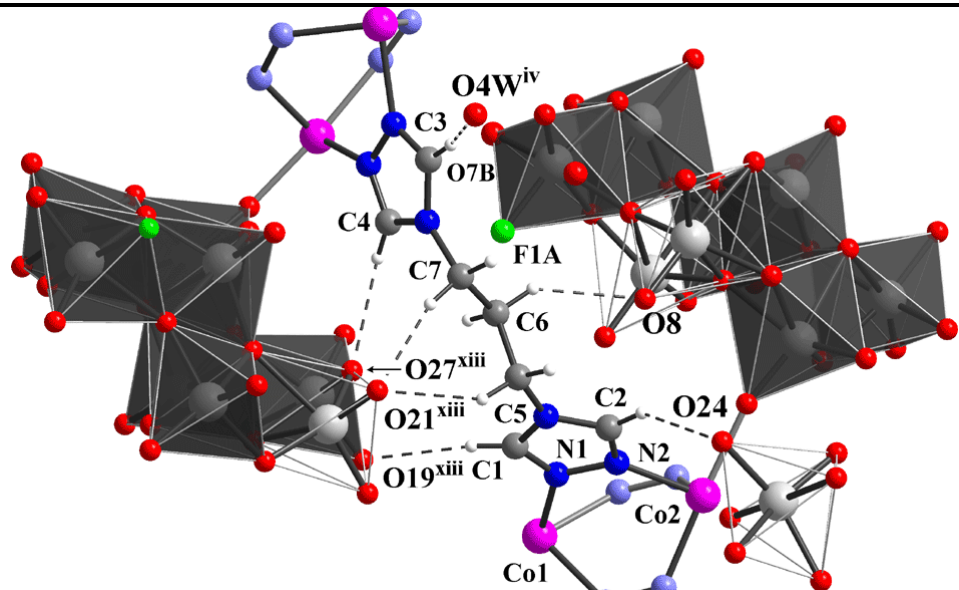
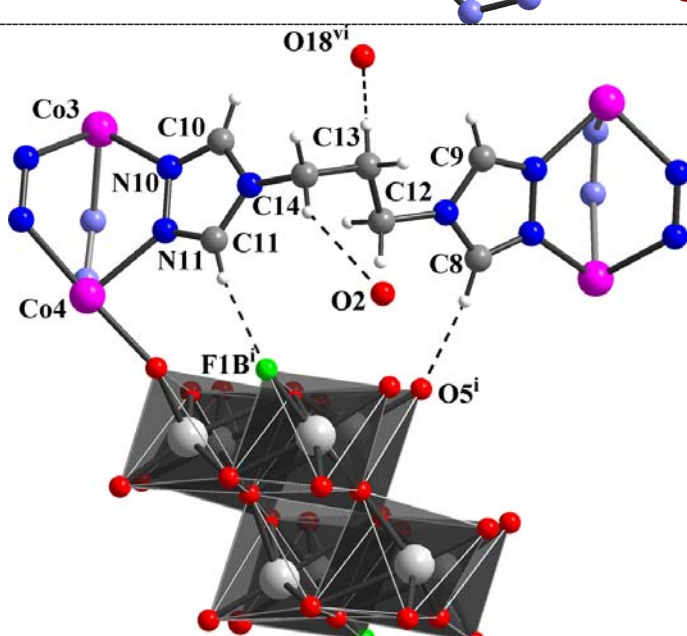


Figure S10. H-bonding patterns ($\text{O}-\text{H}\dots\text{O}$ and $\text{O}-\text{H}\dots\text{F}$) in the crystal structure of **3**. Symmetry codes: (v) $x, y-1, z$; (vi) $-x, -y, -z+1$; (ix) $-x, -y, -z$; (xi) $x, y, z+1$.

a)



b)



c)

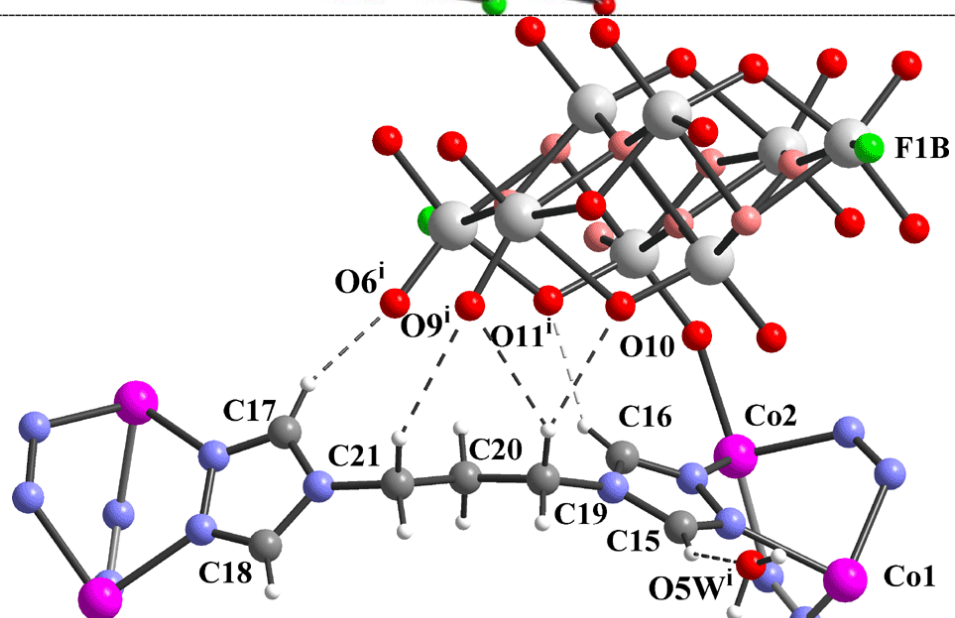


Figure S11. Some weak C-H...O interactions in the crystal structure of **3**. Symmetry codes: (i) $1-x$, $1-y$, $1-z$, (iv) $-x$, $-y+1$, $-z+1$; (vi) $-x$, $-y$, $-z+1$; (xiii) $-x$, $1-y$, $-z$.

a)



b)



Figure S12. Photographs of pink crystalline powder of compound **2** a); and orange powder of compound **3** b).

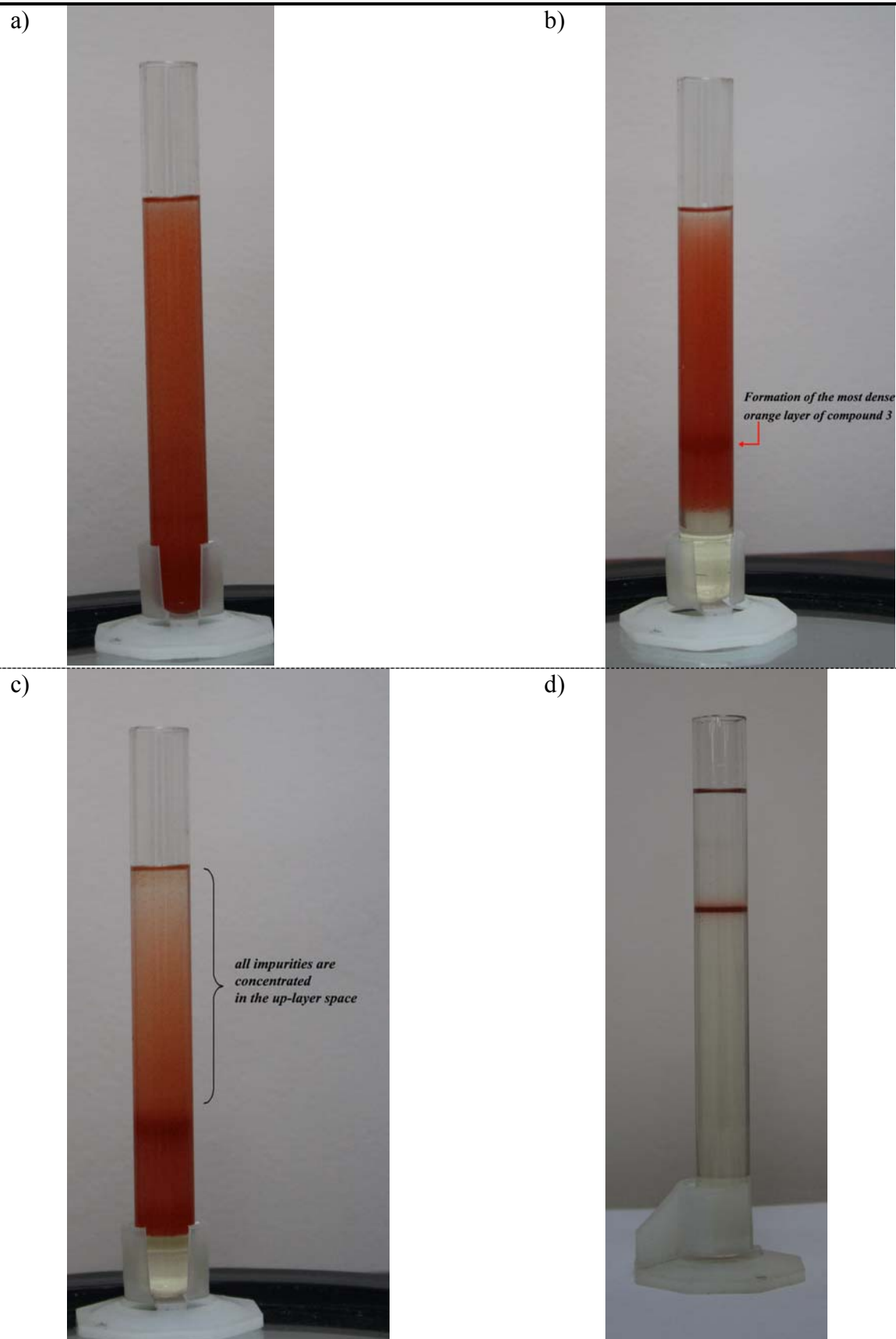


Figure S13. Photographs of a step-wise separation process of compound **3** utilizing a flotation method in a $\text{CHBr}_3/\text{CHCl}_3$ solution: a) the crystalline mixture was immersed in $\text{CHBr}_3/\text{CHCl}_3$; b) the bottom layer contains the most dense compound, i.g., complex **3**; c) the impurities, concentrated in the up-layer space, were removed using a Pasteur pipette. The purification steps (1-3) were repeated over and over again to receive pure phase **3**; d).

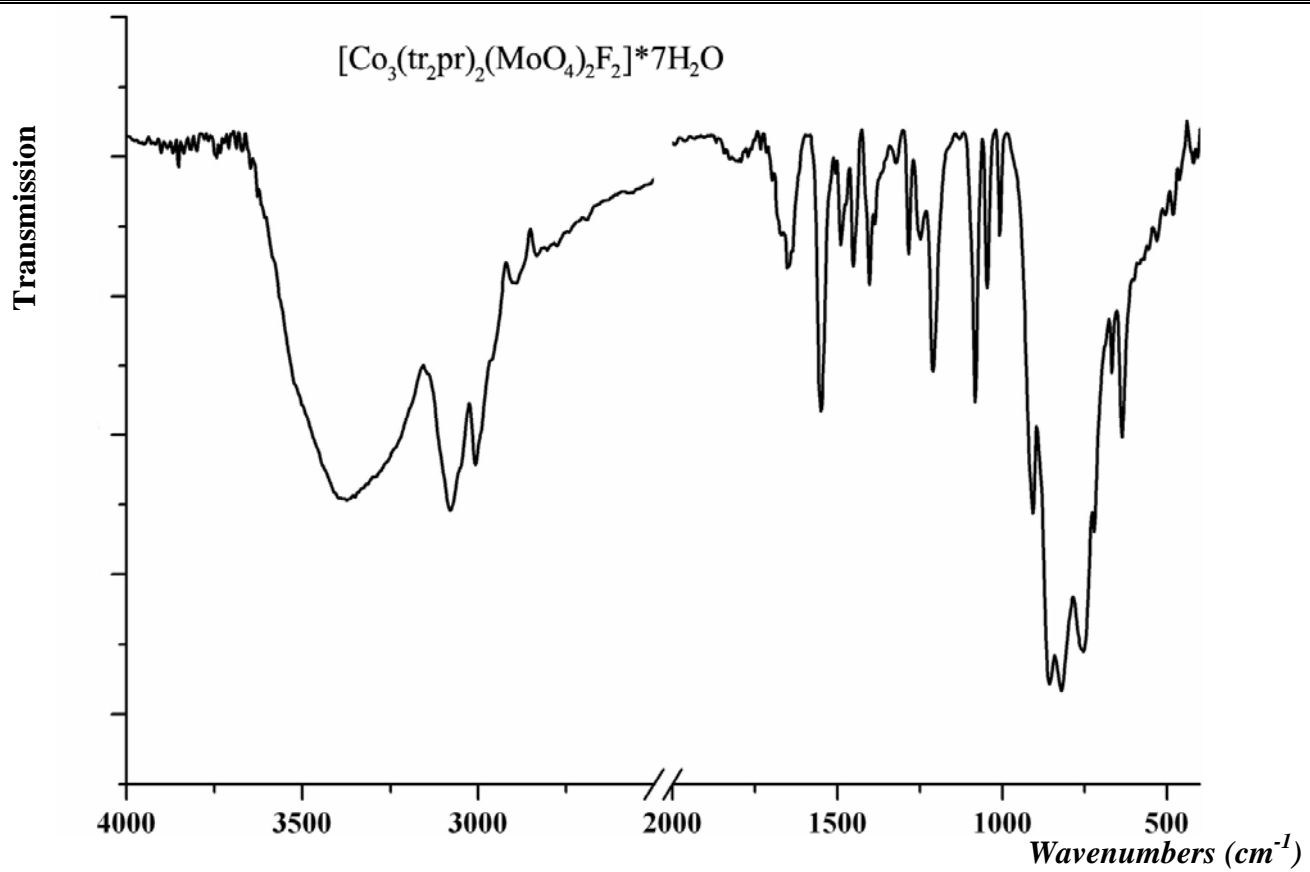


Figure S14. IR spectrum of compound 2.

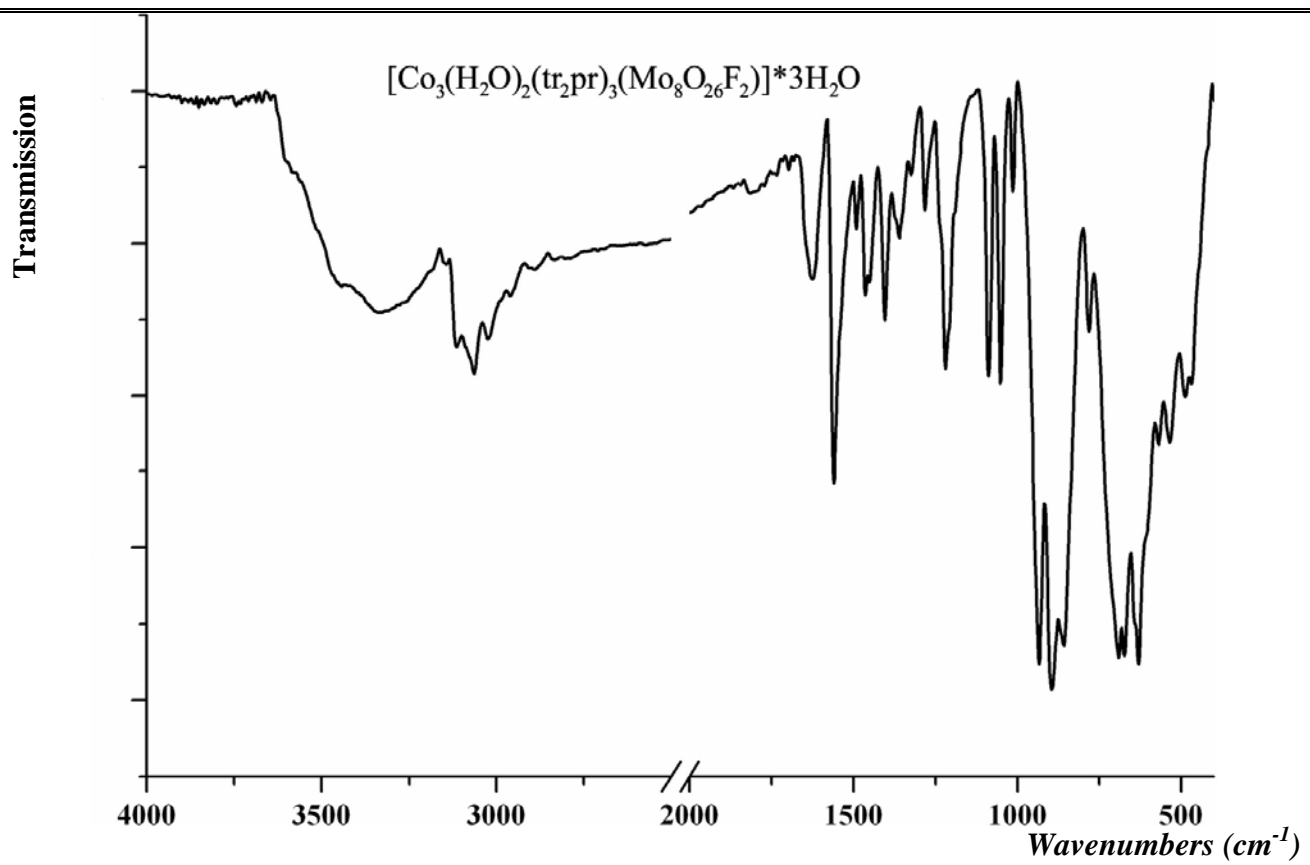


Figure S15. IR spectrum of compound 3.

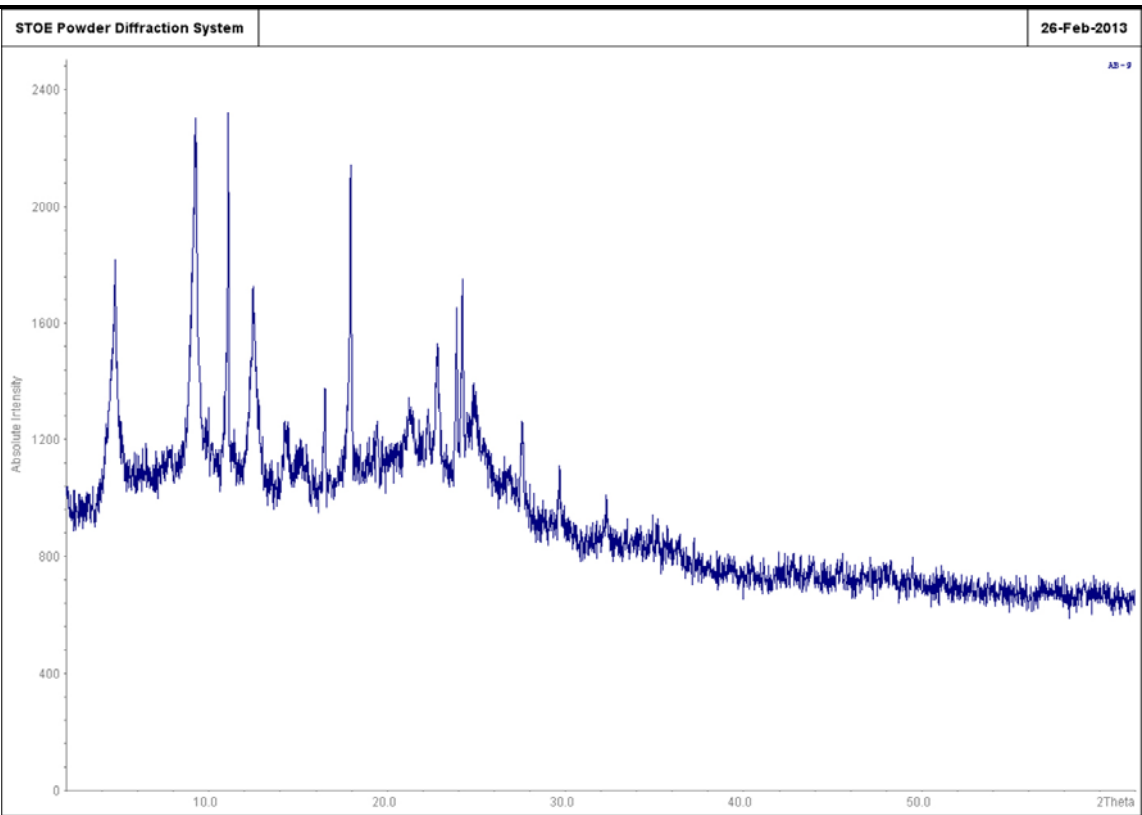


Figure S16. The powder XRD patterns of the unknown phase isolated from hydrothermal reaction of $\text{Co}(\text{OAc})_2 \cdot 4\text{H}_2\text{O}$ (24.9 mg, 0.1 mmol), tr_{2pr} (17.8 mg, 0.1 mmol), MoO_3 (28.8 mg, 0.2 mmol) and 100 μL 22% HF (1.18 mmol) in 5 mL of H_2O .

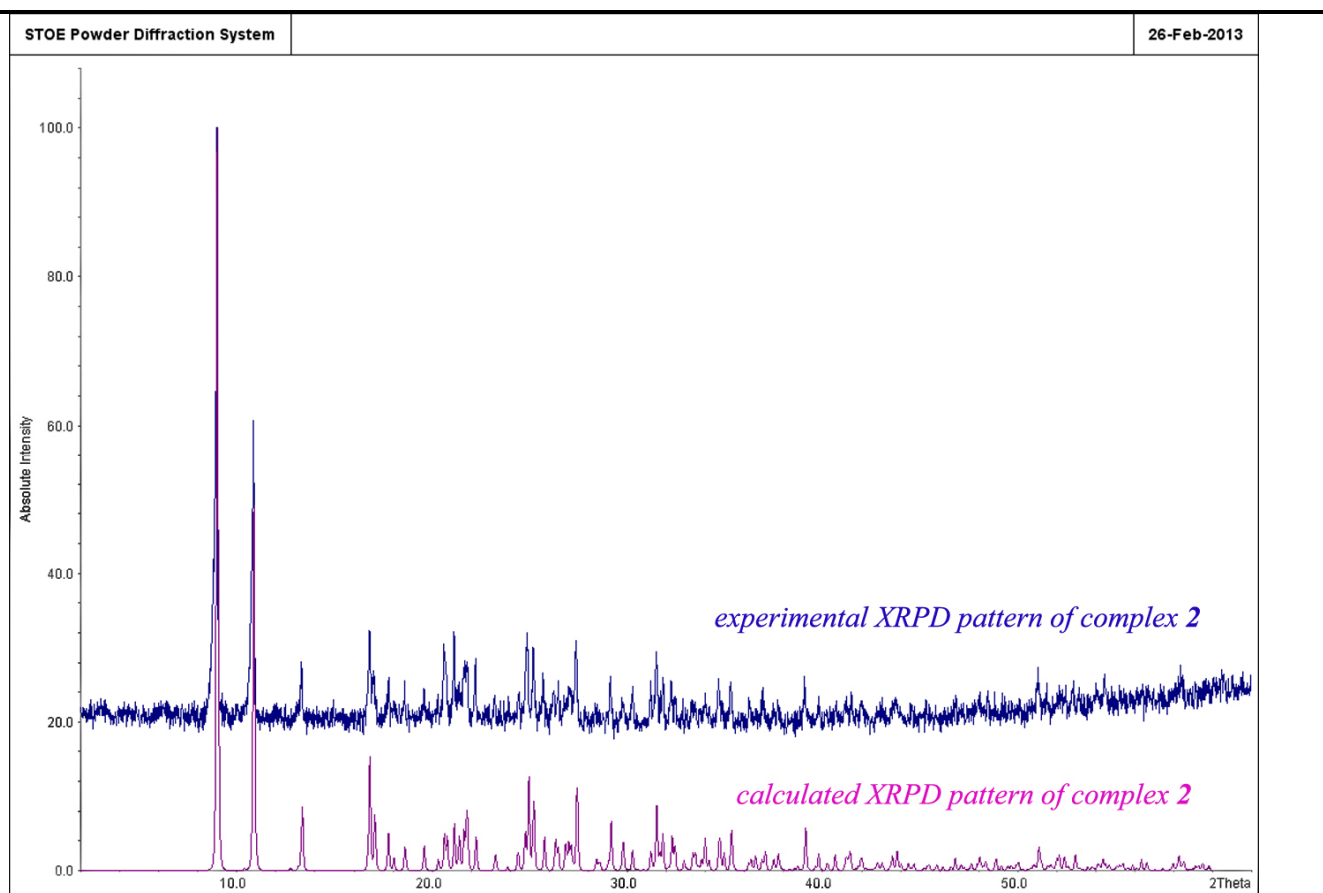


Figure S17. The bulk-phase purity of complex 2 was confirmed by comparing its experimental and simulated XRPD patterns.

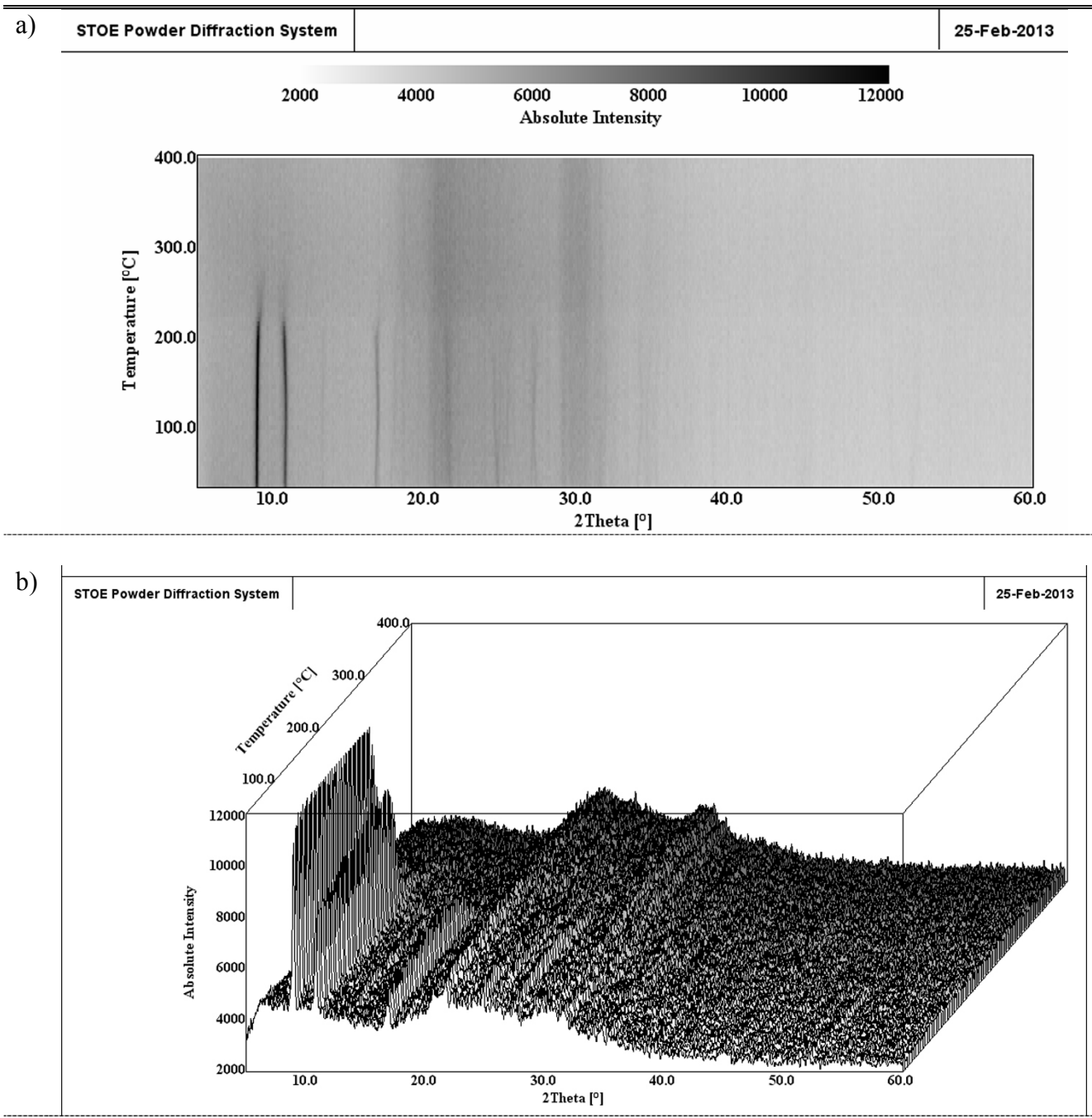


Figure S18. a), b). The 2D and 3D Guinier-Simon diagrams of the TD-XRPD measurements of compound 2.

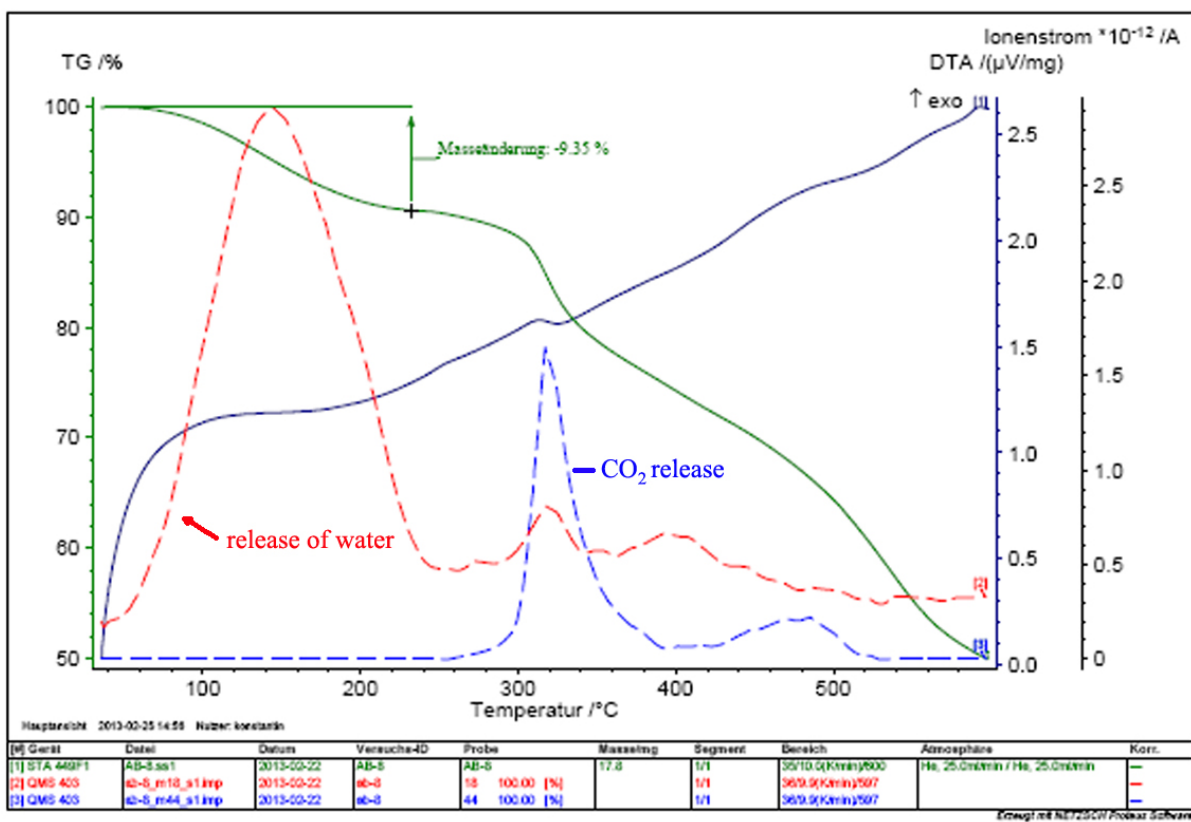


Figure S19. TG-MS analysis of complex 2.

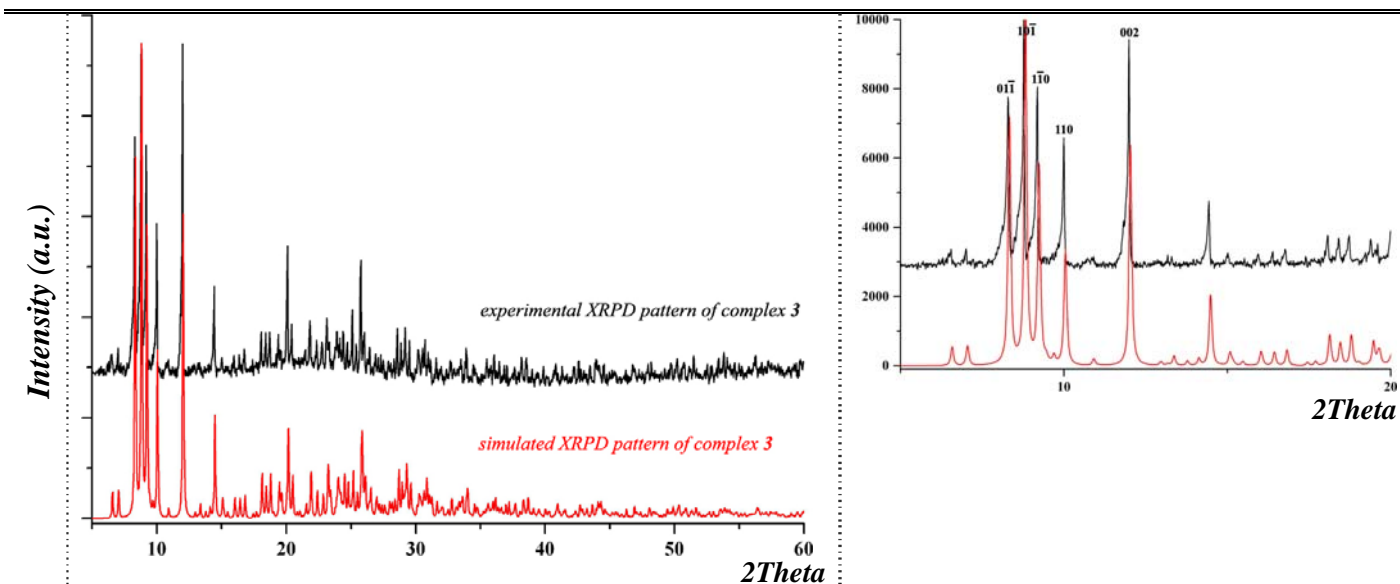


Figure S20. The bulk-phase purity of compound 3 was confirmed by comparing the XRPD patterns with the simulated one.

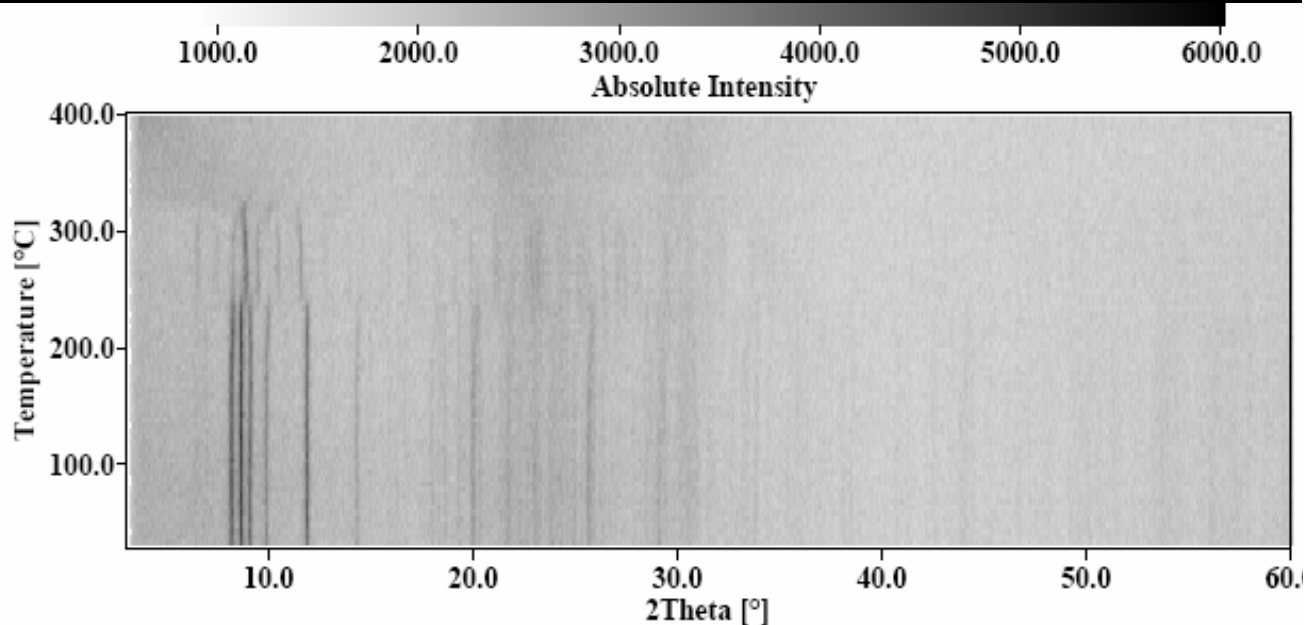


Figure S21. The Guinier–Simon diagram for complex **3** ($2\theta = 5\text{--}60^\circ$) reveals a framework stability up to 240°C .

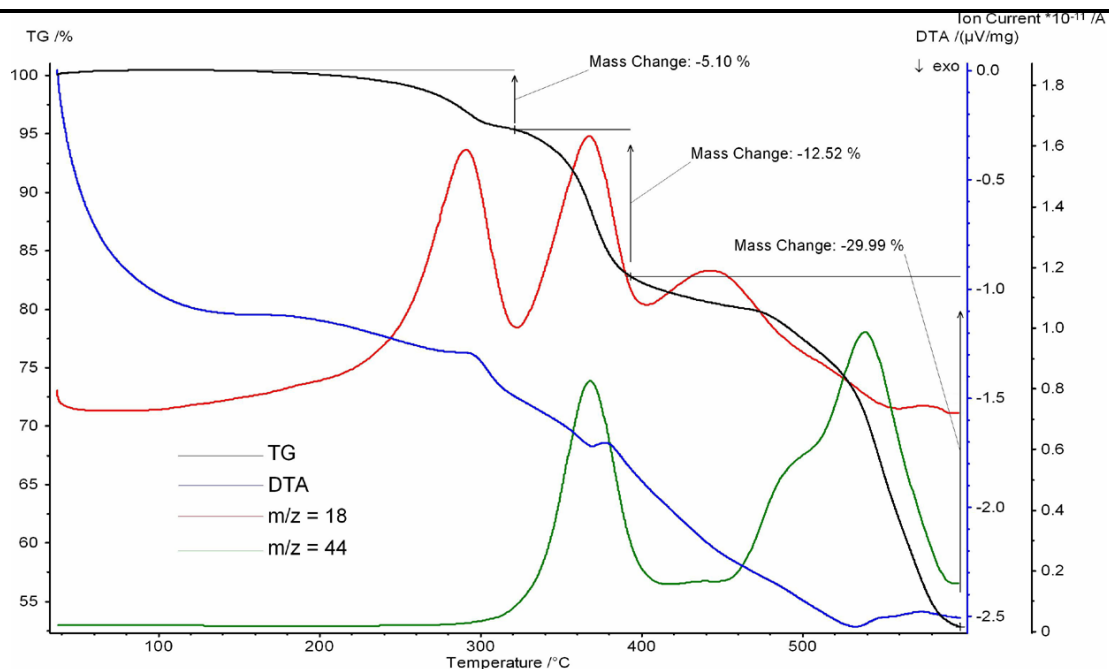


Figure S22. DTA and TGA data showing a weight loss (5.1 %) in the range $165^\circ\text{C} \text{--} 310^\circ\text{C}$, consistent with the removal of five water molecules for $[\text{Co}_3(\text{H}_2\text{O})_2(\text{tr}_2\text{pr})_3(\text{Mo}_8\text{O}_{26}\text{F}_2)] \cdot 3\text{H}_2\text{O}$ (**3**).

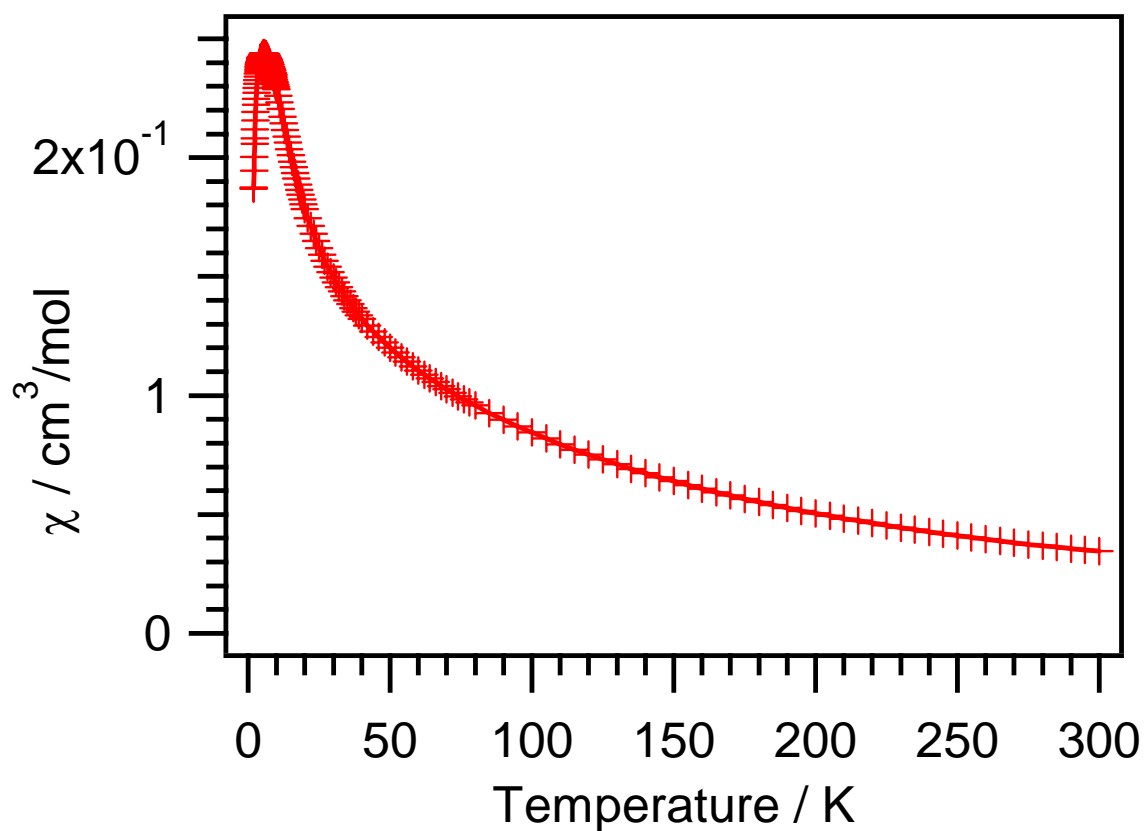


Figure S23. Plot of $\chi_m(T)$ for 2.

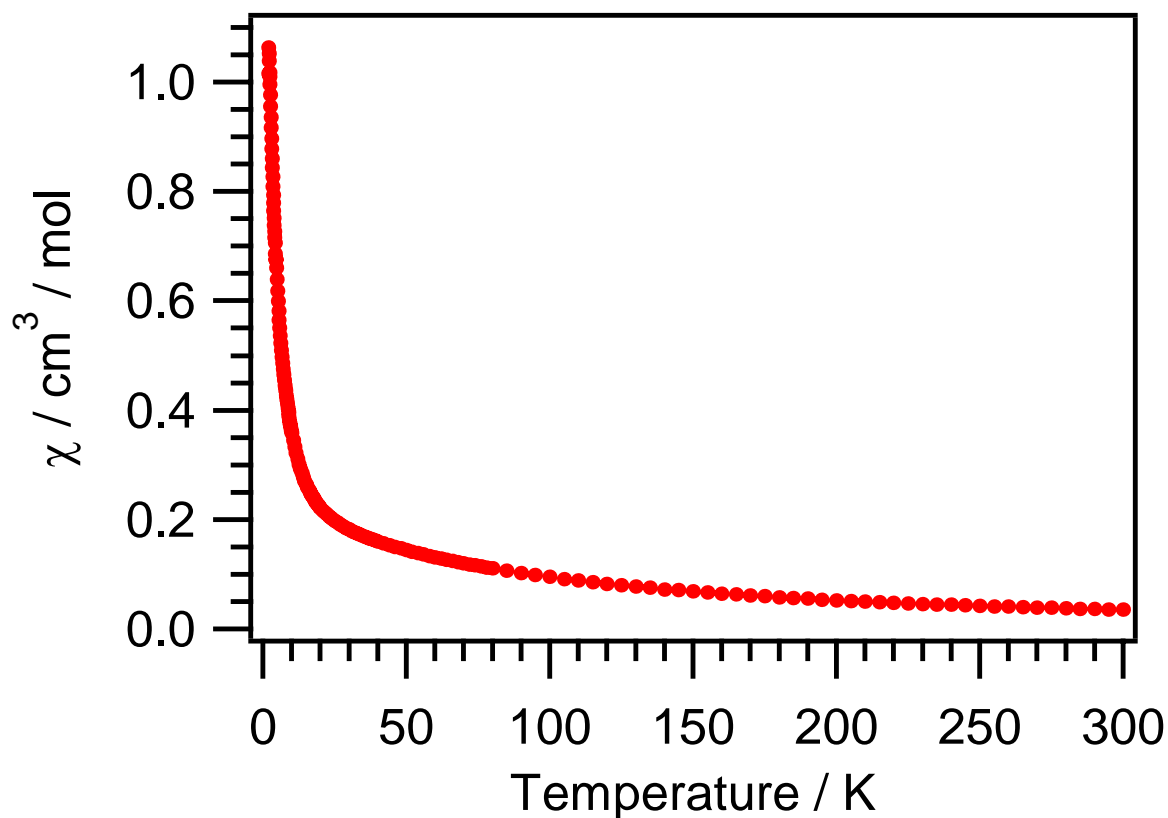


Figure S24. Plot of $\chi_m(T)$ for 3.